Clays and Clay Minerals, Vol. 53, No. 5, 520–527, 2005.

DIFFaX SIMULATIONS OF STACKING FAULTS IN LAYERED DOUBLE HYDROXIDES (LDHs)

A. V. RADHA[1], C. SHIVAKUMARA[2] AND P. VISHNU KAMATH[1,*]

[1] Department of Chemistry, Central College, Bangalore University, Bangalore 560 001, India
[2] Solid State and Structural Chemistry Unit, Indian Institute of Science, Bangalore 560 012, India

Abstract—Carbonate-intercalated layered double hydroxides of Co(II) and Ni(II) with Fe(III) and Al(III) were precipitated under different conditions (pH = 8–12; T = 25–80ºC). All the samples are replete with stacking faults which are not eliminated by post-precipitation hydrothermal treatment (80–180ºC, 18 h). DIFFaX simulations show that the layer stacking sequence of the disordered samples can be generated by a mixture of motifs corresponding to the $3R_1$ and $2H_1$ polytypes. These specific sequences are selected in preference to others because of the need for hydrogen bonding between the intercalated carbonates and hydroxide sheets. Thermodynamic considerations show that faulted crystals have greater stability than ordered crystals. Stacking faults arising from a mixture of $3R_1$ and $2H_1$ motifs, while having the same enthalpy as that of the ordered crystal, nevertheless contribute to thermodynamic stability by enhancing disorder.

Key Words—DIFFaX Simulations, LDHs, Stacking Faults.

INTRODUCTION

Layered double hydroxides (LDHs) are a class of compounds having the general formula $[M(II)_{1-x}M'(III)_x(OH)_2](A^{n-})_{x/n}\cdot mH_2O$, where M(II) = Mg, Fe, Mn, Co, Ni, Cu; M'(III) = Al, Cr, Fe, Ga, In; A^{n-} = Cl^-, CO_3^{2-}, SO_4^{2-}, organic anion; m = 0.66–1.0 (Cavani *et al.*, 1991). The structure of LDHs is derived from that of the mineral brucite, $Mg(OH)_2$. Brucite comprises a hexagonal packing of hydroxyl ions, in which every alternate sheet of octahedral sites is occupied by Mg^{2+} ions, resulting in a stacking of charge-neutral sheets having the composition $[Mg(OH)_2]$ (Oswald and Asper, 1977). When a fraction, x, of the Mg^{2+} ions is substituted isomorphously by a trivalent ion such as Al^{3+}, the sheets acquire a positive charge, with the composition $[Mg_{1-x}Al_x(OH)_2]^{x+}$. Anions and water molecules are incorporated between the sheets for charge neutrality and stability. The compound with M(II) = Mg, M'(III) = Al, x = 0.25, A^{n-} = CO_3^{2-} and m = 0.5 is the mineral hydrotalcite (HT) and it has the formula $Mg_6Al_2(OH)_{16}CO_3\cdot 4H_2O$ (Allmann and Jepsen, 1969). Other LDHs are therefore also called 'hydrotalcite-like' compounds (HTlcs).

The structure of HT can be viewed as a stacking of brucite-like hydroxide sheets intercalated by a layer of anions and water molecules. The basic repeating unit along the c crystallographic axis therefore comprises a brucite-like sheet and an interlayer (Taylor, 1973).

In LDHs, the brucite-like sheets can, in principle, orient in different ways during crystallization. Bookin and Drits (1993) were the first to describe the complete range of theoretically possible stacking sequences among the LDHs. They used the upper case symbols A, B and C to represent hydroxyl ion positions and lower case symbols, a, b and c to describe the cation positions. A typical brucite-like sheet is thus AbC or simply AC, as the cation position is determined by the hydroxyl ion positions. The simplest stacking sequence AC AC ... corresponds to a single layered hexagonal structure similar to that of brucite.

The LDHs are generally synthesized in the laboratory by precipitation reactions (Reichle, 1986) followed by different post-precipitation treatments (Martin *et al.*, 1999; Tichit *et al.*, 2002; Seida *et al.*, 2002; Zhao *et al.*, 2002). The latter are aimed at promoting crystal growth and thereby enhancing crystallite size. Laboratory-synthesized LDH samples generally exhibit excessive and non-uniform broadening of peaks in their X-ray powder diffraction (XRPD) patterns. Such peak broadening is generally attributed to crystallite size effects (Bernard *et al.*, 1996). Belloto *et al.* (1996) ascribed the selective broadening of the 01l peaks to stacking disorders in the LDH of Mg with Ga(III). Drits and Bookin (2001) further refined these ideas and showed that different kinds of stacking disorders produced different peak shapes for the reflections appearing in the mid-2θ region of the X-ray powder diffraction (XRPD) patterns. The peaks in this region correspond to reflections from the 01l/10l planes. In an earlier study of a cohort of $Ni(OH)_2$ samples, we showed that the selective broadening of different families of reflections such as the 00l, hk0 and h0l/0kl are due to different kinds of structural disorders such as interstratification, turbostraticity and stacking faults, respectively (Ramesh *et al.*, 2003).

* E-mail address of corresponding author:
vishnukamath8@hotmail.com
DOI: 10.1346/CCMN.2005.0530508

Naturally occurring minerals, HT and manasseite having the composition $Mg_6Al_2(OH)_{16}CO_3{\cdot}4H_2O$, are found to have the stacking sequences AC CB BA AC ..... and AC CA AC ....., respectively. Bookin and Drits (1993) referred to these polytypes as $3R_1$ and $2H_1$, respectively, to denote the 3-layer and 2-layer periodicity of the respective structures. Furthermore, the $3R_1$ polytype has rhombohedral (R) crystal symmetry, while the $2H_1$ polytype has hexagonal (H) symmetry. In both cases, the interlayer sites have a prismatic coordination. The $3R_1$ sequence is obtained by the translation of successive layers by (2/3,1/3,*z*) which carries A → C, B → A and C → B. The successive layers in $2H_1$ do not have any such simple translational relationship. The $3R_2$ polytype found in a few synthetic LDHs (Newman *et al.*, 2001) has the stacking sequence AC BA CB AC ....., obtained by the translation of successive layers by (1/3,2/3,*z*) which carries A → B, B → C and C → A. The $3R_2$ polytype generates octahedral interlayer sites. The stacking sequence of the brucite-like sheets is mediated by the interlayer. In theory, there are three distinct stacking sequences among the 2-layer LDHs and nine different stacking sequences among the 3-layer LDHs. Each ordered stacking sequence yields a distinct polytype (Bookin and Drits, 1993). Intermixing of these sequences would lead to stacking faults with a multiplicity of motifs, not all of them corresponding to simple translations of successive layers. In this paper, we classify stacking faults into different types and quantify their incidence in carbonate-containing synthetic LDHs.

EXPERIMENTAL

All LDHs were prepared by the method of coprecipitation at constant pH. In a typical preparation, 50 mL of the mixed metal (M^{2+} and M'^{3+}) nitrate solution ($[M^{2+}]/[M'^{3+}] = 3$) were added to a solution of Na_2CO_3 (100 mL) containing three times the stoichiometric requirement of carbonate ions. 1 N NaOH was dispensed simultaneously using a Metrohm Model 718 STAT titrino operating in the pH stat mode. Two separate precipitations of each LDH were affected, one at a constant low (7−8) pH and the other at a constant high (>10) pH. All precipitations were carried out at constant temperature. In each case, the slurry thus obtained was aged at 80ºC for 18 h and then split into two parts. One part was filtered as such, while the other was hydrothermally treated for 24 h in teflon-lined autoclaves filled to 50% capacity. The solids were recovered by filtration, washed copiously to constant pH, and then dried at 80ºC. Numerous samples were prepared and the complete list is given in Table 1 together with the preparation conditions.

All the samples were characterized by XRPD using a Siemens D5005 diffractometer operated with a reflection geometry. Data were collected with CuKα radiation (λ = 1.541 Å) using a continuous scan rate of 2º2θ min^{-1}, which were then rebinned into 2θ steps of 0.05º. The LDHs containing Co and Fe were examined using a Phillips X'pert X-ray diffractometer with a filter to cut off fluorescence radiation under the same conditions. The instrumental broadening of the Bragg peaks is estimated to be 0.15−0.2º2θ in the range 77−28º for the Si standard. Any broadening of the peaks beyond this value is attributed to the sample.

The samples were further characterized by infrared (IR) spectroscopy (Nicolet Model Impact 400D FT IR spectrometer, KBr pellets, resolution 4 cm^{-1}) to verify the presence of intercalated carbonates. For thermogravimetry (TG) (Metler Toledo TGA/SDTA 851[e], Star[e] 7.01) studies, the samples were dried to constant weight at 100ºC in the TG balance to expel adsorbed water before the temperature was ramped (100−800ºC, heating rate 5ºC min^{-1}, flowing air).

DIFFaX SIMULATIONS

The XRPD patterns of different LDHs were computed using the FORTRAN-based code, DIFFaX (Treacy *et al.*, 2000). In the DIFFaX formalism (Treacy *et al.*, 1991), a crystalline solid is treated as a stacking of planes of

Table 1. Precipitation conditions used for the synthesis of different LDH samples.

LDH system	pH	*T* (ºC)	Post-precipitation treatment	% water Observed[a]	% water Expected[b]
Co-Fe-CO_3	7	25	80ºC, 18 h	33.3[c]	32.2[c]
Co-Fe-CO_3	10	25	80ºC, 18 h	32.3[c]	32.2[c]
Co-Al-CO_3	8	23	80ºC, 18 h	14.9	13.8
Co-Al-CO_3	10	24	80ºC, 18 h	13.6	13.8
Ni-Fe-CO_3	7	60	80ºC, 18 h	10.9	12.0
Ni-Fe-CO_3	7	60	150ºC, 24 h	14.0	12.0
Ni-Fe-CO_3	10	60	80ºC, 18 h	10.8	12.0
Ni-Al-CO_3	>12	40	80ºC, 18 h	12.1	13.9
Ni-Al-CO_3	>12	40	180º C, 24 h	11.2	13.9

[a] Estimated from TG data for the dehydration step; [b] calculated as per the water content used in DIFFaX simulations; [c] estimated total weight loss from TG data.

https://doi.org/10.1346/CCMN.2005.0530508 Published online by Cambridge University Press

atoms, interconnected by appropriate stacking vectors. Within the DIFFaX formalism, it is necessary that the *c* crystallographic axis be defined along the stacking direction. The XRPD pattern is then simulated by integrating the diffraction intensities layer by layer. The details of the DIFFaX simulations of LDHs are given elsewhere (Thomas *et al*., 2004) and summarized here.

The LDH layer comprises a brucite-like hydroxide sheet and an interlayer of carbonate anions and water molecules, having the composition MO_2 and $C_{x/2}O_z$, respectively, (H atoms are ignored, x = trivalent ion content). The oxygen atoms of the carbonate ions and water molecules occupy a single set of sites (Taylor, 1973), so that of the z O atoms, $3x/2$ belong to the carbonate ions and $z-3x/2$ correspond to the water content of the interlayer. By varying this latter value, the water content can be varied. The position coordinates of all the atoms are obtained from the International Crystal Structure Database [ICSD No. 6296]. This corresponds to the mineral hydrotalcite and the same layer is adopted for all other LDHs as well. This assumption is reasonable, as most LDHs and their polytypes have the same layer as the building block. They crystallize in different space groups because of the differences in the stacking sequences. By explicitly specifying the coordinates of all symmetry-related atoms, we declare the point group symmetry of the crystal as unknown. The DIFFaX code then computes the Laue symmetry. The cell parameters were obtained from the XRPD patterns (a = 2 d_{110} Å; c = 6 d_{006} Å). The calculated reflections were broadened by using a Lorentzian line shape. The full width at half maximum (FWHM) value chosen for the Lorentzian was obtained from the width of the 110 reflection. Depending on the sample, this varied from 0.3 to 0.7°2θ. In the as-prepared LDH of Ni with Al, the broadening was so excessive that a successful simulation could be realized only with a Lorentzian of FWHM of 1.4°2θ. Broadening of the 110 reflection in excess of the instrumental factors is ascribed to crystallite-size effects as this reflection is largely unaffected by structural disorder (Ramesh *et al*., 2003). For layered materials, crystallite size is defined along the $a-b$ plane as 'disc diameter'. A small disc diameter broadens the 110 reflection (Ramesh *et al*., 2003). Choosing the FWHM of the 110 reflection for the Lorentzian line profile obviates the need to explicitly include crystallite size in the simulation. As DIFFaX is not a profile-refinement procedure, but relies only on a visual match between the simulated and observed patterns, a Lorentzian line shape has been found to be adequate. Any broadening of the peaks in the experimental pattern in excess of the broadening of the 110 reflection is attributed to structural disorder arising out of stacking faults. Different stacking fault motifs are simulated by the appropriate choice of the stacking vector and layer description. The use of the stacking vector (2/3,1/3,1/3) generates the perfectly ordered $3R_1$ polytype while the use of (1/3,2/3,1/3) generates the $3R_2$ polytype. A mixture of $3R_1$ and $3R_2$ motifs can be generated by the simultaneous use of the stacking vectors (2/3,1/3,1/3) and (1/3,2/3,1/3) with different probabilities. The $2H_1$ polytype is generated by defining two different layers AC and CA and then stacking them one atop another using the stacking vector (0,0,1/2). A mixture of $3R_1$ and $2H_1$ motifs can be generated using AC and CA layers. As stated earlier, beginning with an AC layer, the $3R_1$ motif is generated by using the stacking vector (2/3,1/3,1/3). However while beginning with a CA layer, the $3R_1$ motif is generated by using the vector (1/3,2/3,1/3), leading to the sequence CA AB BC CA ..... This is an enantiomorph of the AC CB BA AC ..... sequence mentioned earlier (Drits and Bookin, 2001). The percentage incidence of the $3R_1$ motifs is then given by probabilities $P_{ACCB} = P_{CAAB}$. The percentage incidence of the $2H_1$ motifs is given by the probabilities $P_{ACCA} = P_{CAAC}$. The probabilities of the stacking vectors are varied by hand until a good visual match between the simulated and experimental patterns is obtained. The goodness of the visual match is based on obtaining an approximate match of the: (1) peak positions (within ±0.1°2θ); (2) FWHM values (within ±0.1°2θ); and (3) intensities (within ±5%) of the simulated peaks with those in the observed pattern. To facilitate this comparison, the experimental and simulated patterns are overlain and the difference plotted.

RESULTS AND DISCUSSION

In Figure 1 we compare the simulated XRPD patterns of the $2H_1$, $3R_1$ and $3R_2$ polytypes in the Co-Fe LDH system. Three regions of the patterns can be observed. The low-angle (10–25°2θ) region contains the reflections arising from the basal, 00*l* planes. As the thickness of the brucite-like sheet and the interlayer is the same in all the polytypes, the basal reflections appear at identical

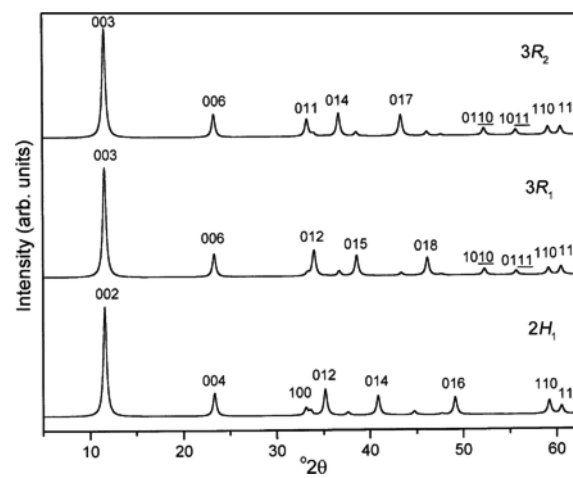

Figure 1. Simulated XRPD patterns of $2H_1$, $3R_1$ and $3R_2$ polytypes.

https://doi.org/10.1346/CCMN.2005.0530508 Published online by Cambridge University Press

Table 2. 2θ values of the three most intense lines observed in mid-2θ region of different polytypes.

	°2θ		
hkl	$2H_1$	$3R_1$	$3R_2$
100	33.1		
011			33.3
012	35.15	34.0	
013			
014	40.85		36.7
015		38.6	
016	49.1		
017			43.35
018		46.15	

angles in all the simulations. The high-angle (>60°2θ) region contains reflections of the *hk*0 and *hkl* family. The former is affected most by intralayer ordering. As the same layer is used in all the polytypes, these reflections also do not change significantly in different simulations. Different stacking sequences affect the positions and relative intensities of the *h*0*l*/0*kl* reflections appearing in the mid-2θ (30−55°2θ) region. The three polytypes can be distinguished from each other by the three most intense lines in this region (see Table 2).

In Figures 2 and 3 the XRPD patterns of the Co-Fe LDH precipitated at low (7) and high (10) pH, respectively, are shown. The following features are observed: (1) The intensity of the 006 reflection relative to the 003 reflection is much higher in the experimental pattern than in the simulated pattern of the pure polytype. (2) The peaks in mid-2θ region can be indexed to the 01*l* (*l* = 2, 5, 8) reflections, expected of the $3R_1$ polytype. (3) The 01*l* reflections are non-uniformly broadened, the FWHM of the 018 being the highest, 1.0°2θ and the 012 being the narrowest, 0.5°2θ. In addition, the relative intensities of the 015 and 018 reflections are less in the experimental pattern than in the simulated pattern of the pure $3R_1$ polytype. (4) The broadening of the 01*l* reflections is greater in the sample precipitated at high pH than that precipitated at low pH.

As explained by Thomas *et al.* (2004), the relative intensity of the 006 reflection is proportional to the electron density of the interlayer and can be corrected by increasing the intercalated water content. The non-uniform broadening of the 01*l* reflections is because of stacking faults. The most general stacking faults can be generated by the incorporation of layers randomly translated by (1/3,2/3,*z*) or (2/3,1/3,*z*). This amounts to randomly mixing the $3R_1$ and $3R_2$ motifs. Such a faulted crystal generates both octahedral and prismatic interlayer sites. Other ways of generating stacking faults involve the random insertion of CA, AB or BA layers together with their corresponding interlayer into the $3R_1$ polytype. These generate motifs corresponding to the $2H_1$, $2H_2$ and $2H_3$ polytypes, respectively (Bookin and Drits, 1993). Insertion of the CA layer generates prismatic interlayer sites, while insertion of the AB layer generates only octahedral interlayer sites. Insertion of the BA layer generates both octahedral and prismatic interlayer sites. Of these, we select for consideration the insertion of the CA layer, as the carbonate anions are known to prefer prismatic interlayer sites (Taylor, 1973).

We show in Figures 4 and 5 the changes brought about in the mid-2θ region of the XRPD pattern of the $3R_1$ polytype by the incorporation in different proportions of the $3R_2$ and $2H_1$ motifs respectively. Incorporation of $3R_2$ motifs causes a drastic broadening of the 01*l* (*l* = 2, 5, 8) reflections, until only three broad

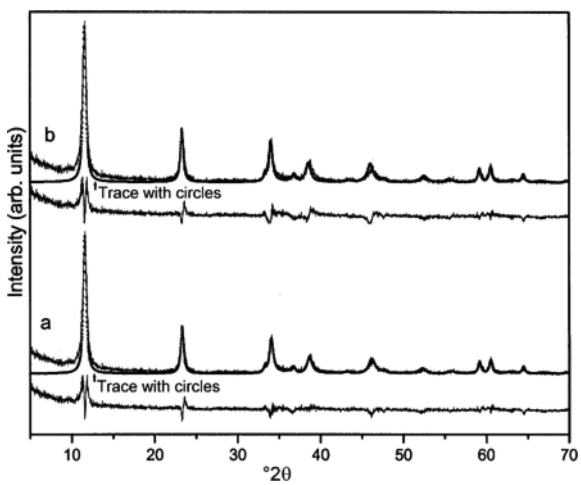

Figure 2. XRPD pattern of Co-Fe-CO_3 LDH (solid line) precipitated at pH 7 compared with the DIFFaX simulation (open circles) incorporating (a) 15% $2H_1$ motifs and (b) 10% $3R_2$ motifs in the $3R_1$ polytype. The difference curves are also plotted.

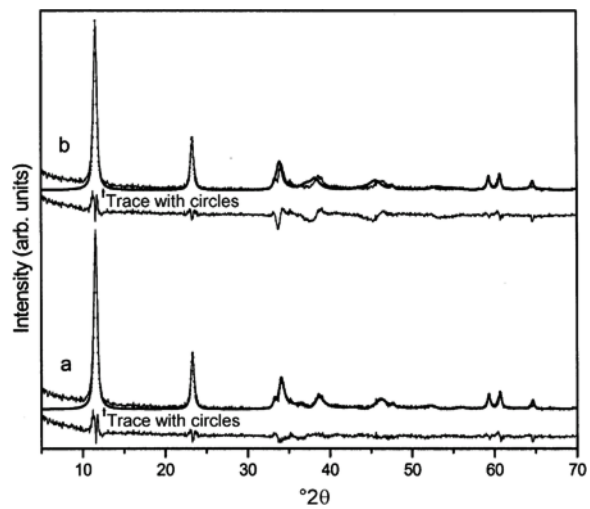

Figure 3. XRPD pattern of Co-Fe-CO_3 LDH (solid line) precipitated at pH 10 compared with the DIFFaX simulation (open circles) incorporating (a) 30% $2H_1$ motifs and (b) 30% $3R_2$ motifs in the $3R_1$ polytype. The difference curves are also plotted.

https://doi.org/10.1346/CCMN.2005.0530508 Published online by Cambridge University Press

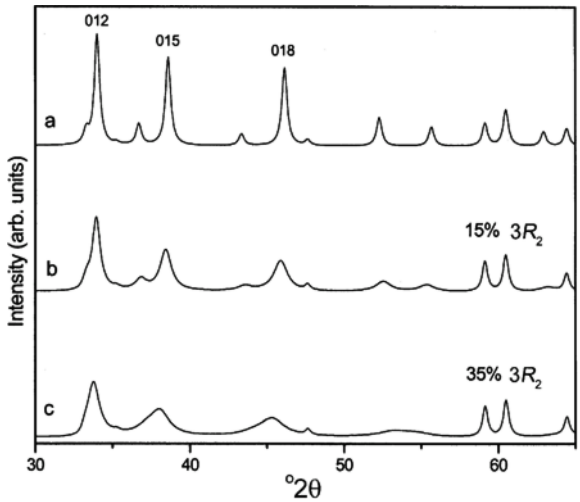

Figure 4. Simulated XRPD patterns of mixtures of $3R_1$ and $3R_2$ motifs in various proportions: (a) 0%, (b) 15% and (c) 35% $3R_2$ in the $3R_1$ polytype.

features remain in the mid-2θ region. Incorporation of the $2H_1$ motifs retains many of the minor reflections in the simulated pattern of the faulted crystal.

With this understanding, we attempted to simulate the patterns of the Co-Fe LDH. The results are presented in Figures 2 and 3. Incorporation of 1.35 O atoms in the interlayer yielded the observed ratio of the I_{006}/I_{003}. Of this, 0.375 O atoms belong to the carbonate ions and 0.975 O belong to intercalated water, to yield a formula $Co_6Fe_2(OH)_{16}(CO_3)\cdot 7.8H_2O$. This composition was verified by thermogravimetric studies. The LDH of the Co with Fe decomposes in a single step. The observed total weight loss was 33.3% (800ºC) while that expected on the basis of the above formula is 32.2%. This match is satisfactory. All other LDHs decompose in two steps. The low-temperature (100–250ºC) weight loss corresponds to dehydration resulting from the loss of intercalated water, while the high temperature (>250ºC) weight loss corresponds to the complete decomposition of the hydroxide to yield the oxide residue. The low-temperature weight loss is used to estimate the intercalated water content, which is then compared with the water content required to simulate the relative intensities of the basal reflections. Incorporation of 1.2 O in the interlayer, of which 0.825 O atoms belong to intercalated water, yielded the best simulations for all the LDHs other than the Co-Fe LDH. This intercalated water content also matches the TG data (see Table 1).

The broadening of the peaks in the mid-2θ region for the sample precipitated at pH 7 could be simulated both by the inclusion of $2H_1$ motifs (15%) (Figure 2a) as well as by the inclusion of $3R_2$ motifs (10%) (Figure 2b). On the other hand, the sample precipitated at pH 10 was simulated better by the inclusion of 30% $2H_1$ motifs (Figure 3a). The best solution obtained by the inclusion of $3R_2$ motifs (30%) (Figure 3b) is also shown. Attempts to order the Co-Fe LDH by hydrothermal treatment failed as the samples were found to decompose at $T \geqslant 150$ºC. At lower temperatures, no ordering was observed.

The mid-2θ region of the XRPD patterns of the Co-Al LDH precipitated at low pH (8) could be simulated by incorporating 20% of $2H_1$ motifs (see Figure 6a), while that of the sample precipitated at high pH (10) could be simulated by incorporating 55% of $2H_1$ motifs (see Figure 6b). In this system, incorporation of $3R_2$ motifs yielded less satisfactory results.

In conclusion, among the Co-based LDHs, a more ordered product is obtained at a lower pH. When the proportion of stacking faults is small (<20%), these simulations do not distinguish unequivocally between

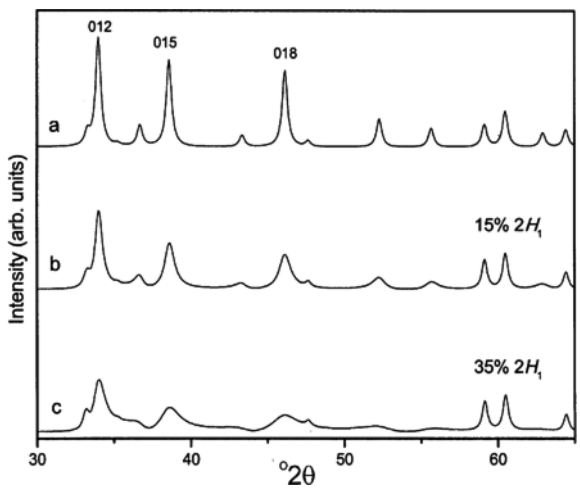

Figure 5. Simulated XRPD patterns of mixtures of $3R_1$ and $2H_1$ motifs in various proportions: (a) 0%, (b) 15% and (c) 35% $2H_1$ in the $3R_1$ polytype.

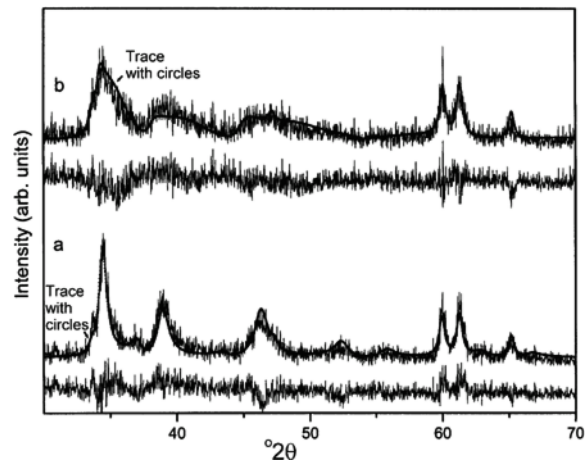

Figure 6. XRPD patterns in the mid-2θ region of the Co-Al-CO_3 LDH (solid line) precipitated at (a) pH 8 and (b) pH 10 compared with the DIFFaX simulations (open circles) incorporating 20% $2H_1$ and 55% $2H_1$ motifs in the $3R_1$ polytype, respectively. The difference curves are also plotted.

https://doi.org/10.1346/CCMN.2005.0530508 Published online by Cambridge University Press

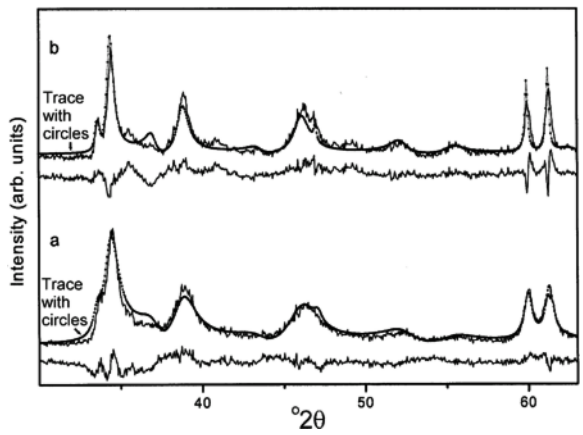

Figure 7. XRPD patterns in the mid-2θ region of Ni-Fe-CO_3 LDH (solid line) precipitated at pH 7 (a) before and (b) after hydrothermal treatment compared with the DIFFaX simulations (open circles) incorporating 35% $2H_1$ and 25% $2H_1$ motifs in the $3R_1$ polytype, respectively. The difference curves are also plotted.

the $2H_1$ motifs and $3R_2$ motifs. At higher pH, the products exhibit a high proportion of stacking faults corresponding to the inclusion of $2H_1$ motifs in the $3R_1$ polytype.

LDHs of Ni with Fe and Al

One of the well known ways of eliminating structural disorder is by hydrothermal treatment (Rabenau, 1985). Hydrothermal treatment has been used to bring about the gel → crystallite conversions among the layered hydroxides (Fievet and Figlarz, 1975). We therefore attempted to eliminate the stacking faults by subjecting freshly precipitated slurries of the Ni-Fe LDH to prolonged hydrothermal treatment (150ºC, 18 h). We show in Figure 7 the mid-2θ region of the XRPD patterns of the Ni-Fe LDH before and after hydrothermal treatment. The XRPD pattern of the as-prepared LDH could be simulated satisfactorily by a combination of 65% $3R_1$ + 35% $2H_1$ motifs (Figure 7a) while the hydrothermally treated sample exhibited 25% of the $2H_1$ motif (Figure 7b). The other difference in the two simulations was the choice of the Lorentzian. While a FWHM of 0.6º2θ was chosen for Figure 7a, a FWHM of 0.2º2θ was chosen for Figure 7b. A narrower line shape is reflective of a larger crystallite size in the hydrothermally treated sample. From these results we conclude that hydrothermal treatment facilitates crystal growth, without introducing structural order.

Similar results were also obtained in the Ni-Al system (data not shown). The complete results of the simulations of all the LDHs are summarized in Table 3.

Verma and Krishna (1966) discussed in detail the structural and thermodynamic aspects governing polytypism. The same arguments are extended here to faulted crystals. Thermodynamically, any phase having the lowest free energy is stable under the given set of conditions. The free energy of any phase has both enthalpy and entropy components, of which the former dominates over the latter, especially at low temperatures. The enthalpy of a system essentially arises out of bond formation in the first, second and higher coordination spheres in decreasing order of importance. Among LDHs, the following interactions are expected to contribute to the enthalpy of the system: (1) bonding within the brucite sheet; (2) bonding within the interlayer; (3) ionic bonding between the positively charged brucite sheet and the negatively charged interlayer; and (4) hydrogen bonding between the brucite sheet and the interlayer atoms.

Since all the polytypes within a given LDH system comprise the same brucite sheet and interlayer, the contribution of factors 1 and 2 above remains the same for all polytypes. Factor 3 depends solely on the positive charge on the layer. As long as this value is maintained constant, its contribution is expected to remain invariant not only for different polytypes, but also across different LDH systems. Therefore, the chief determinant for the preference of one polytype over the others is the hydrogen bonding between the brucite sheet and the interlayer. Different polytypes generate different types of sites in the interlayer. The requirement of hydrogen bonding dictates the nature of interlayer sites and thereby selects certain specific stacking sequences among the range of possibilities. The carbonate anion used in the present study is known to intercalate with its plane perpendicular to the *c* axis. Such an orientation is compatible with a prismatic interlayer site to maximize the extent of H bonding (Taylor, 1973) and thereby maximize the enthalpy of the system. Of all the two- and three-layer polytypes, only two, *i.e.* $3R_1$ and $2H_1$, incorporate purely prismatic interlayer sites. Other polytypes contain either octahedral or a mixture of octahedral and prismatic interlayer sites. Consequently, from the enthalpy point of view, the $3R_1$ and $2H_1$ polytypes would have comparable stability.

When two polytypes have comparable enthalpies, the entropy factor comes into play. Ordered structures are

Table 3. Results of DIFFaX simulations of the different LDHs.

LDH	$3R_1$ (%.)	$2H_1$ (%.)	$3R_2$ (%.)	Point group
Co-Fe-CO_3 pH7	85	15	–	6/*mmm*
	90	–	10	$\bar{3}m$
Co-Fe-CO_3 pH10	70	30	–	6/*mmm*
	70	–	30	$\bar{3}m$
Co-Al-CO_3 pH8	80	20	–	6/*mmm*
Co-Al-CO_3 pH10	45	55	–	6/*mmm*
Ni-Fe-CO_3	65	35	–	6/*mmm*
Ni-Fe-CO_3 150ºC	75	25	–	6/*mmm*
Ni-Al-CO_3	50	50	–	6/*mmm*
Ni-Al-CO_3 180ºC	50	50	–	6/*mmm*

https://doi.org/10.1346/CCMN.2005.0530508 Published online by Cambridge University Press

obviously not favored from entropy considerations. Disorders that do not affect the enthalpy contribute to thermodynamic stability. Stacking faults belong to this category of disorders as they do not disturb the coordination sphere of the metal ions. Restricting the stacking faults to the $3R_1$ and $2H_1$ motifs further ensures that the strength of the hydrogen bonding is also not affected. Thus the faulted crystals, while having the same enthalpy as the ordered crystals, nevertheless have a greater thermodynamic stability due to the stacking disorders. The stacking faults are incorporated during precipitation and once incorporated cannot be eliminated even by hydrothermal treatment.

Despite their many similarities, the $3R_1$ and $2H_1$ polytypes differ from one another in the packing of their cations. The cation stacking sequence is b a c b a c .... in the former, while it is b b b .... in the latter. It is unclear how strong these interactions are as the cations are four neighbors removed from each other along the *c* axis. The $3R_2$ polytype with similar cation packing to that in $3R_1$ is a strong contender for stability from this point of view. Consequently the $3R_2$ polytype has been realized in the Mg-Al system. In an earlier paper we proposed the intergrowth of $3R_1$ and $3R_2$ motifs to explain the broadening of reflections in the Mg-Al system (Thomas *et al.*, 2004). However, the $3R_2$ polytype provides only octahedral sites, which do not favor hydrogen bonding with the interlayer carbonates.

The effect of the different cation packings on the XRPD pattern become apparent when the cations are strong scatterers as in the Co-Fe and Ni-Fe system. In highly disordered preparations of these LDHs, DIFFaX simulations distinguish the intergrowth of $3R_1$ and $2H_1$ motifs from the intergrowth of $3R_1$ and $3R_2$ motifs.

In situations where simulations are unable to distinguish between different kinds of stacking faults, we can take recourse to the point group symmetry of the faulted crystals. Verma and Krishna (1966) related thermodynamic stability directly to the point group symmetry; the crystal with a higher symmetry being more stable. The DIFFaX code generates a $\bar{3}m$ Laue group for the ordered $3R_1$ and $3R_2$ polytypes. The $2H_1$ polytype yields the 6/*mmm* Laue group. While, in general, structural disorder destroys the point group symmetry of a crystal, stacking faults are different. Thus, incorporation of turbostratic disorder and interstratification generates the trivial $\bar{1}$ diffraction symmetry (Ramesh *et al.*, 2005). In a trigonal crystal, however, introduction of stacking faults along the stacking direction, also the *c* axis, retains the axis of symmetry (Verma and Krishna, 1966). The Laue symmetry computed for a crystal with a mix of $3R_1$ and $3R_2$ motifs is $\bar{3}m$, while the incorporation of $2H_1$ motifs with $3R_1$ generates the Laue symmetry 6/*mmm* (Table 3), showing that the latter has greater thermodynamic stability.

CONCLUSIONS

Ordered polytypes are thermodynamically unstable among the LDHs and most preparations crystallize replete with stacking faults that contribute to thermodynamic stability by maximizing the entropy. Further, hydrogen bonding considerations limit the stacking faults to the $3R_1$ and $2H_1$ motifs among the carbonate-containing LDHs.

ACKNOWLEDGMENTS

The authors thank the Department of Science and Technology of the Government of India for financial support. AVR thanks the University Grants Commission, GOI, for the award of a Senior Research Fellowship (NET).

REFERENCES

Allmann, R. and Jepsen, H.P. (1969) Die struktur des hydrotalkits. *Neues Jahrbuch für Mineralogie Monatshefte*, **12**, 544–551.

Bellotto, M., Rebours, B., Clause, O., Lynch, J., Bazin, D. and Elkaim, E. (1996) A reexamination of hydrotalcite crystal chemistry. *Journal of Physical Chemistry*, **100**, 8527–8534.

Bernard, M.C., Cortes, R., Keddam, M., Takenouti, H., Bernard, P. and Senyarich, S. (1996) Structural defects and electrochemical reactivity of β-Ni(OH)$_2$. *Journal of Power Sources*, **63**, 247–254.

Bookin, A.S. and Drits, V.A. (1993) Polytype diversity of the hydrotalcite-like minerals I. Possible polytypes and their diffraction features. *Clays and Clay Minerals*, **41**, 551–557.

Cavani, F., Trifiro, F. and Vaccari, A. (1991) Hydrotalcite-type anionic clays: preparation, properties and applications. *Catalysis Today*, **11**, 173–301.

Drits, V.A. and Bookin, A.S. (2001) Crystal structure and X-ray identification of layered double hydroxides. Pp. 39–92 in: *Layered Double Hydroxides: Present and Future* (V. Rives, editor). Nova Science, New York.

Fievet, F. and Figlarz, M. (1975) Preparation and study by electron microscopy of the development of texture with temperature of a porous exhydroxide nickel oxide. *Journal of Catalysis*, **39**, 350–356.

Martin, M.J.S., Villa, M.V. and Camazano, M.S. (1999) Glyphosate-hydrotalcite intercalation as influenced by pH. *Clays and Clay Minerals*, **47**, 777–783.

Newman, S.P., Jones, W., O'Connor, P. and Stamires, N. (2001) Synthesis of the 3R$_2$ polytype of a hydrotacite-like mineral. *Journal of Materials Chemistry*, **12,** 153–155.

Oswald, H.R. and Asper, R. (1977) Bivalent metal hydroxides, Pp. 71–140 in: *Preparation and Crystal Growth of Materials with Layered Structures*, vol. **1** (R.M.A. Lieth, editor). D. Reidel Publishing Company, Dordrecht, The Netherlands.

Rabenau, A. (1985) The role of hydrothermal synthesis in preparative chemistry. *Angewandte Chimie International, English Edition*, **24**, 1026–1040.

Ramesh, T.N., Jayashree, R.S. and Kamath, P.V. (2003) Disorder in layered hydroxides: DIFFaX simulation of the X-ray powder diffraction patterns of nickel hydroxide. *Clays and Clay Minerals*, **51**, 570–577.

Ramesh, T.N., Kamath, P.V. and Shivakumara, C. (2005) Correlation of structural disorder with the reversible discharge capacity of nickel hydroxide electrode. *Journal of Electrochemical Society*, **152**, A806–A810.

Reichle, W.T. (1986) Synthesis of anionic clay minerals

(mixed metal hydroxides, hydrotalcites). *Solid State Ionics*, **22**, 135–141.

Seida, Y., Nakano, Y. and Nakamura, Y. (2002) Crystallization of layered double hydroxides by ultrasound and the effect of crystal quality on their surface properties. *Clays and Clay Minerals*, **50**, 525–532.

Taylor, H.F.W. (1973) Crystal structure of some double hydroxide minerals. *Mineralogical Mag*azine, **39**, 377–389.

Thomas, G.S., Rajamathi, M. and Kamath, P.V. (2004) DIFFaX simulations of polytypism and disorder in hydrotalcite. *Clays and Clay Minerals*, **52**, 693–699.

Tichit, D., Rolland, A., Prinetto, F., Fetter, G., Martinez-Ortiz, M.J., Valenzuela, M.A. and Bosch, P. (2002) Comparison of the structural and acid-base properties of Ga- and Al-containing layered double hydroxides obtained by microwave irradiation and conventional ageing of synthesis gels. *Journal of Materials Chemistry*, **12**, 3832–3838.

Treacy, M.M.J., Newsam, J.M. and Deem, M.W. (1991) A general recursion method for calculating diffracted intensities from crystals containing planar faults. *Proceedings of the Royal Society, London*, **A433**, 499–520.

Treacy, M.M.J., Deem, M.W. and Newsam, J.M. (2000) *Computer code DIFFaX*, Version 1.807.

Verma, A.R. and Krishna, P. (1966) *Polymorphism and Polytypism in Crystals*. John Wiley and Sons, Inc., New York.

Zhao, Y., Li, F., Zhang, R., Evans, D.G. and Duan, X. (2002) Preparation of layered double-hydroxide nanomaterials with a uniform crystallite size using a new method involving separate nucleation and aging steps. *Chemistry of Materials*, **14**, 4286–4291.

(*Received 2 November 2004; revised 16 April 2005; Ms. 977; A.E. James E. Amonette*)